Supplement of Geosci. Model Dev., 17, 2299–2324, 2024
https://doi.org/10.5194/gmd-17-2299-2024-supplement

Geoscientific Model Development
Open Access
EGU

Supplement of

Optimising CH_4 simulations from the LPJ-GUESS model v4.1 using an adaptive Markov chain Monte Carlo algorithm

Jalisha T. Kallingal et al.

Correspondence to: Jalisha T. Kallingal (jalisha.theanutti@nateko.lu.se)

S1 Active peat column properties

The acrotelm layers have a porosity (por_{acro}) of 0.98, while the catotelm layers, assumed to be made of older, denser peat, have a porosity (por_{cato}) of 0.92. Each layer consists of constant proportions of peat and varying proportions of water (F_{water}), ice (F_{ice}), and air (F_{air}), all with distinct thermal characteristics given in Table S1. The active column is covered by a maximum of five snow layers, with a depth that can reach 10 m water equivalent, and five extra padding layers that extend to a depth of 48 m. These layers are thermally active, but, hydrologically inactive, with the bottom three layers having thermal properties of bedrock.

S1.1 Peat temperature

Temperature in each active peat layer is calculated daily by solving the heat diffusion equation;

$$\frac{\partial T}{\partial t} = \frac{\partial}{\partial x}\left(D(z,t)\frac{\partial T}{\partial z}\right) \tag{1}$$

where *T* represents the temperature of the soil at a a specific depth z (*m*) and time *t*, while *D(z,t)* $(m^2 s^{-1})$ denotes the thermal diffusivity at depth z and time *t*, defined as:

$$D(z,t) = \frac{K(z,t)}{C(z,t)} \tag{2}$$

where *K(z,t)* $(W\, m^{-1} K^{-1})$ represents the thermal conductivity, and *C(z,t)* $(Jm^{-3}K^{-1})$ represents the soil layer component's heat capacity (Table S1), each at a depth z and time *t*.

Table S1. Heat capacities ($10^6 Jm^{-3}K^{-1}$) and thermal conductivities ($Wm^{-1}K^{-1}$) of the soil layer components. The values are originally adopted from, Wania et al. (2009a, b); Bonan et al. (2002); Granberg et al. (1999); and Chadburn et al. (2015).

Component	Heat capacity	Thermal conductivity
Peat	0.58	0.06
Water	4.18	0.57
Ice	1.94	2.2
Air	0.0012	0.025
Bedrock	2.1	8.6

Water plays a major role in the wetland's soil temperature because of the dynamics of latent heat during its phase change (Wania et al. (2009a, b)). When temperature changes over time and depth, $T(z,t)$ in the soil, the values of F_{water} and F_{air} also change due to phase change, with a similar spatial (0.1 *m*) and temporal (1 *day*) resolution.

S1.2 Peat hydrology

As mentioned above, it is assumed that the catotelm layers remain saturated permanently with no inflow or outflow, but to maintain saturation, water is added to these layers on a daily basis, if necessary. This is because PFTs such as graminoid species can absorb water from the catotelm layers via their roots.

Thus, the model updates only the daily water content in acrotelm, and predicts the wtd, where 0 <= *wtd* <= 300 *mm*, i.e., *wtd* is positive below the surface, and standing water is not permitted. Each day the change in total volume of water in acrotelm (V) is calculated as:

$$\Delta V = run_{on/off} + rain_{melt} - evap - aet_{acro} - runoff_{acr0} \tag{3}$$

where *evap* represents the amount of water that gets evaporate from the bare peat soil fraction, $rain_{melt}$ represents the daily amount of water input to the patch as rainfall and/or snowmelt, $runoff_{acro}$ is the runoff from the acrotelm and aet_{acro} is the transpiration from the acrotelm based on the root distributions in the acrotelm layers.

Once the total volume of water is determined, the *wtd* in the acrotelm is assumed to be linear in the first top interval (0-0.1 *m*) and constant below this depth and up to the lower limit of the acrotelm, i.e., 0.1-0.3 *m* (Granberg et al., 1999). Hence if 0.1 *m* >= *wtd* >= 0 the *wtd* is calculated as:

$$wtd = \sqrt{\frac{3\left(por_{acro} \times 0.3 - V\right)}{2 \times a_z}} \tag{4}$$

And for *wtd* > 0.1 *m* the *wtd* is calculated as:

$$wtd = \frac{1.5 \times \left(por_{acro} \times 0.3 - V\right)}{por_{acro} - f_{surfmin}} \tag{5}$$

where $f_{surfmin}$ = 0.00025 is the surface minimum fractional water content in m^3/m^3, por_{acro} is the porosity in the acrotelm and a_z = por_{acro} - $f_{surfmin}/0.1$ is the gradient in the uppermost 0.1 *m* suction interval, The water profile of soil $\theta(z)$ in each layer of 0.1 *m* is calculated as,

$$\theta(z) = \min\left(por_{acro}, \theta_{surf} + \left(por_{acro} - \theta_{surf}\right)\left(\frac{z}{wtd}\right)^2\right) \tag{6}$$

where the θ_{surf}, the surface water content is calculated as,

$$\theta_{surf} = max(f_{surfmin}, por_{acro} - wtd \times a_z) \tag{7}$$

Once $\theta(z)$ in each 0.01 *m* layer is known, the average of ten 0.01 *m* layers is used to calculate the F_{water} in each of the three 0.1 *m* sublayers of the acrotelm, which will then used for calculating the thermal properties, i.e., for the soil temperature calculations described above.

S1.3 Peatland PFTs

Table S2 provides the properties of four types of PFTs that can exist on peatland stands. The model includes a generic herbaceous cushion lichen moss PFT (pCLM), low deciduous and evergreen shrubs (*pLSE* and *pLSS*, respectively). The leaf area index (*LAI*) of nearby trees or shrubs is a limiting factor on PFTs. The model sets a maximum LAI limit of 2 m^2m^{-2} for mosses and graminoids, and exceeding this limit leads to increased shade mortality. Similarly a daily desiccation stress factor [0,1] and an inundation stress factor are also introduced in the model. A desiccation stress factor of 1 indicates that there is no stress, whereas a value of 0 signifies complete suspension of photosynthetic activity for that day (applies only to mosses and graminoids). Inundation stress factor is implemented to control assimilation when the rooting zone experiences anoxia. The model restricts PFTs with a maximum *wtd* threshold and the number of inundated days ($inund_{days}$) they can tolerate before assimilation (Table S2).

S1.4 SOM dynamics and daily decay rates

Table S2. Important parameter values used for defining Wetland PFTs. Here the WTD_{inun} (*mm*) is the maximum *wtd* threshold, and $inund_{days}$ (*days*) that are the number of days wetland PFTs can tolerate inundated conditions.

PFT	WTD_{inun}	$inund_{days}$	Aerenchyma	Photosynthesis stress due to lower *wtd*
pLSE, pLSS	250	5	No	N/A
Sphagnum moss	50	15	No	0.3
C3 graminoids	N/A	N/A	Yes	0.0
pCLM	200	10	No	N/A

The Soil organic matter (SOM) scheme in the LPJ-GUESS is adopted from the CENTURY model (Parton, 1996; Smith et al., 2014) with eleven distinct pools of different carbon : nitrogen (C : N) stoichiometry and base decay rates (Fig. 01). The decomposition rates in the acrotelm, which is often wet and sometimes saturated, are slow. In the catotelm, where conditions are permanently saturated and anaerobic, decomposition rates are particularly slow (Frolking et al., 2001, 2010). The decomposition rate for wetlands is computed daily for each pool using the following equation:

$$\frac{dC_j}{dt} = -k_{j,max} f(T) f(W) f(S) . C_j \tag{8}$$

where C_j is the carbon content in pool *j*, $k_{j,max}$ is maximum decay rate, $f(T_{soil}), f(W)$ (from here on-wards called $Rmoist$) and $f(S)$ are dimensionless scalars between $0-1$ related to soil temperature, soil moisture and soil fractional silt plus clay content (*S*) respectively. Considering the negligible soil fractional silt plus clay content in peat ($S = 0$), $f(S) = 1$. From the parameter sensitivity test conducted by Wania et al. (2010), the value of $Rmoist$ in LPJ-GUESS is adopted as 0.4 for carbon in the acrotelm. After the acrotelm soil carbon is fully established, which involves a peat layer 0.3 m deep with a carbon density of 25 *kg C* m^{-3}, corresponding to a total soil carbon amount of 7.5 *kg C* m^{-2} across all pools, the value of $Rmoist$ will be reduced from the weighted average 0.4 to 0.025, hence in anaerobic catotelm conditions the moisture response $Rmoist_{an}$ = 0.025.

S2 Twin experiments: Parameter convergence

Figure S1 shows the thinned trace plots resulted from all four experiments in scenario 1 of the twin experiments. In most of the experiments, except for CH_4/CO_2 and λ_{root}, at least two of the parameters have completely converged to their z_{true} values. Two experiments performed reasonably well for λ_{root}, whereas none of them could converge to z_{true} for CH_4/CO_2. Figure S2 shows the posterior correlations between the parameters in Experiment 1 of scenario 1 for the twin experiment. The majority of the parameters, except for a few, have shown no strong positive or negative correlations with each other.

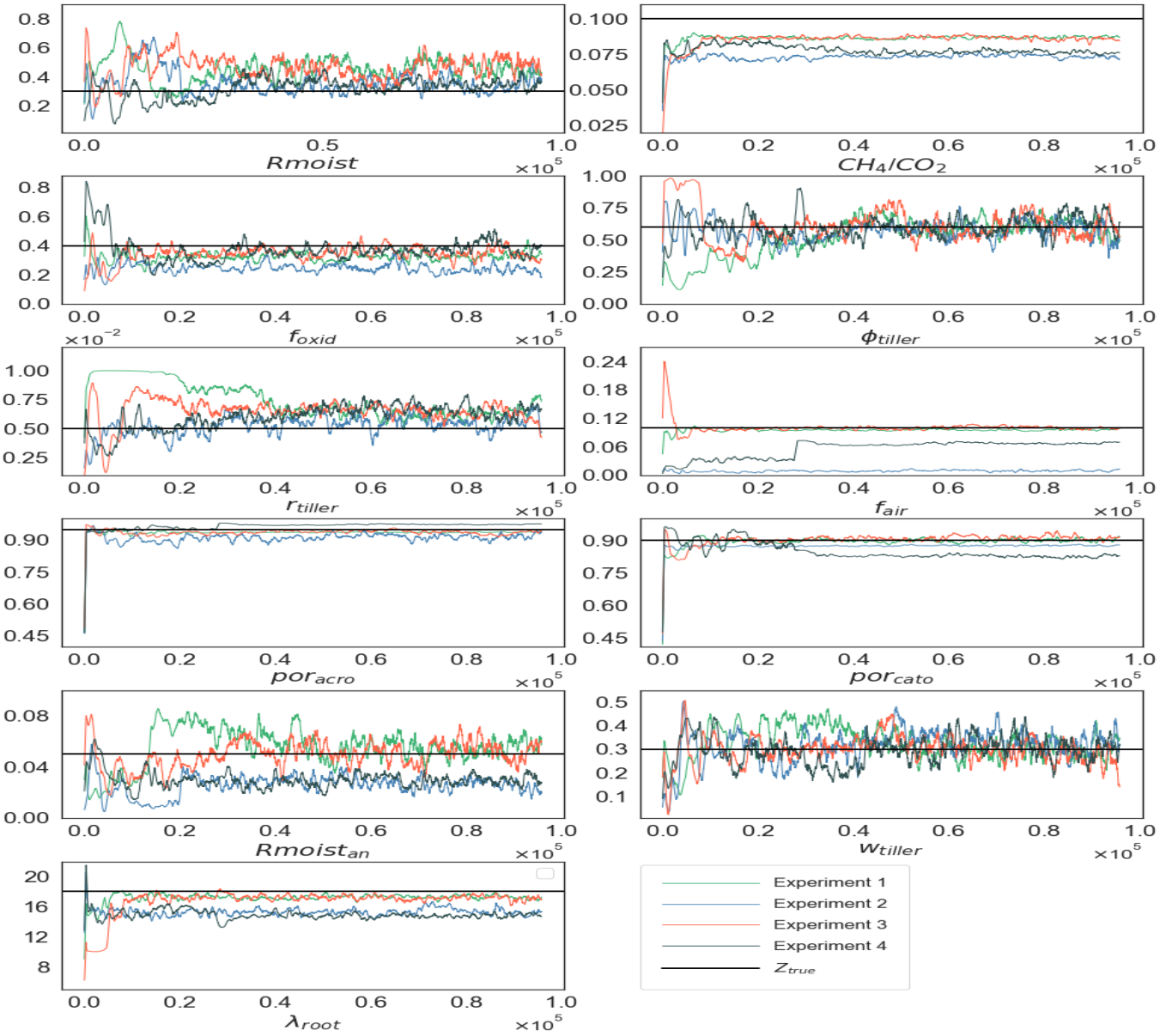

Figure S1. Thinned trace plots resulted from the scenario 1. The black vertical lines shows the z_{true} values used to generate the twin observation and the trace plots in each colour represents different experiments.

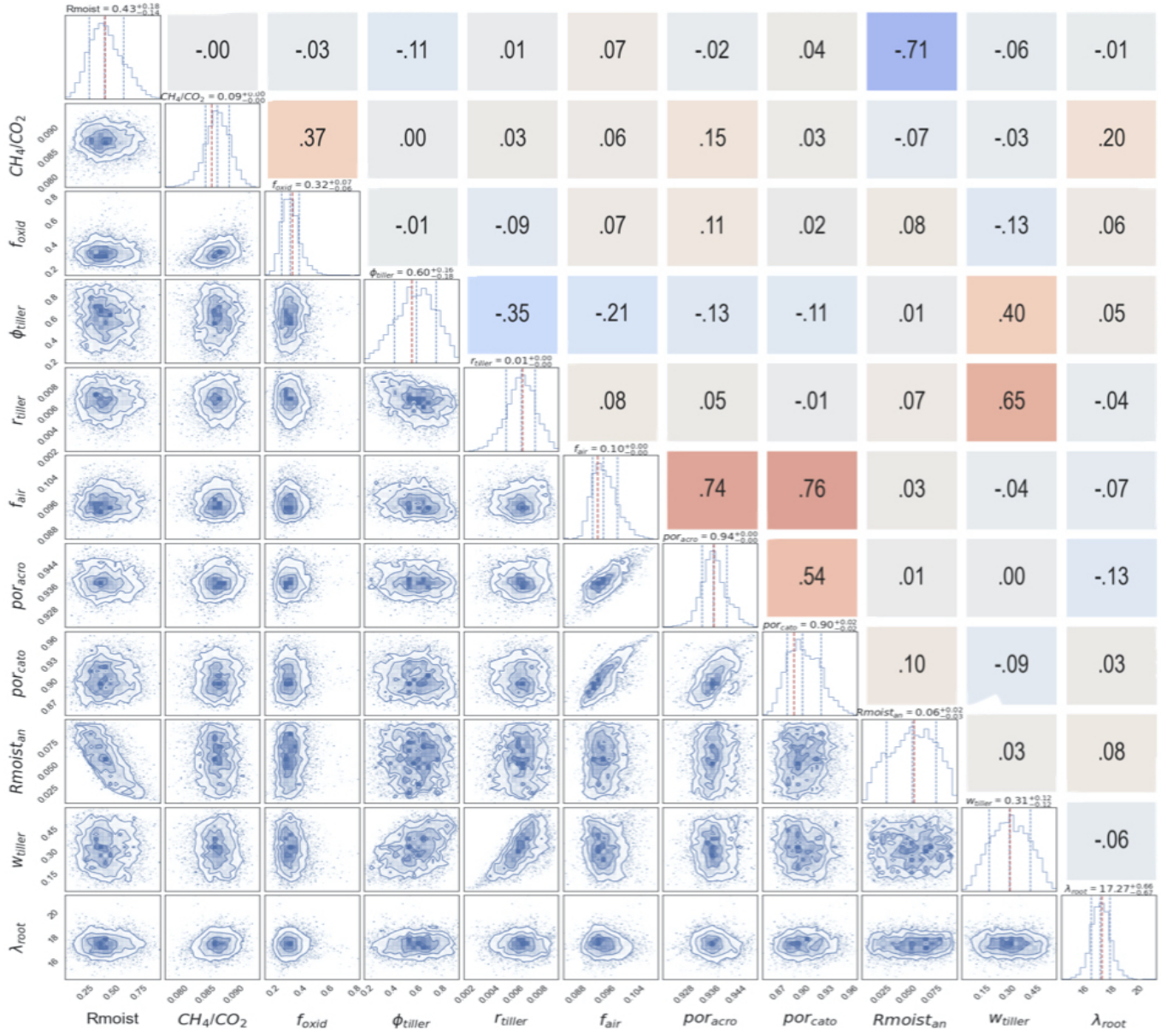

Figure S2. A posteriori correlations between the parameters from the GRaB-AM twin optimisation. Blue and red colour in the upper triangle represents the strong negative and positive correlations respectively. The numerical labels on the upper triangle are the values of Pearson's correlation coefficient. The panels on the diagonal show the 1-D histogram for each model parameters with a dashed red vertical line to indicate their modes. The vertical blue lines are the 0.16, 0.5 and 0.84 quantiles of the distributions. The lower triangle represents the two-dimensional marginal distributions of each parameter with contours to indicate 1σ, 2σ and 3σ confidence levels and the blue dots in the plots are the posterior parameter values of GRaB-AM chain. Ranges of the distributions are labeled on the left and bottom of the figure.

S3 Correlation between the driving environmental variables and the CH_4 residuals

After optimisation, the model still exhibited some misfit to the observations, particularly displaying systematic underestimation for the years 2010, 2012, and 2013 (see Sect. 4.4 of the paper). To investigate the potential reasons, we conducted a correlation

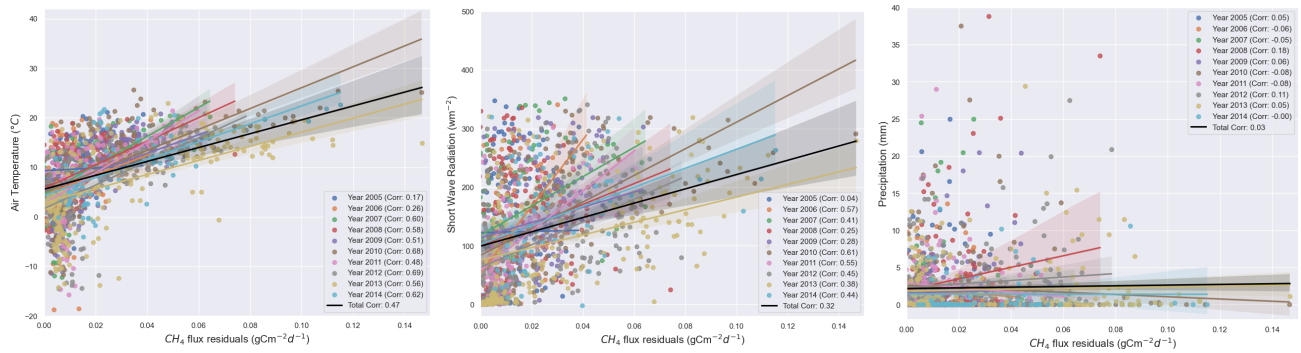

(a) Temperature vs. CH_4 residuals (b) Short-wave vs. CH_4 residuals (c) Precipitation vs. CH_4 residuals

Figure S3. Correlation estimation between the input variables of LPJ-GUESS and the residuals of the observations and optimised simulations of CH_4 flux.

analysis between the observed and optimised model residuals of CH_4 and the input environmental variables of LPJ-GUESS, as shown in Fig. S3. In the years 2010 and 2012, we observed a high correlation between the flux and swr (0.61 and 0.45 respectively) as well as air temperature (0.68 and 0.69 respectively). In 2013, while the correlation between the flux and swr was not as high (0.38), the flux exhibited a strong correlation (0.56) with air temperature. No significant correlations were found between the flux and precipitation.

S4 Other related flux components

Figure S4 shows the time series of observed and simulated soil temperature and *wtd* from 2005 to 2015. The observed soil temperature aligns well with the model summer simulations. During the winter in Siikaneva, the observed soil temperature remains close to zero. However, the model simulates much lower soil temperatures in the winter, occasionally showing unusual spikes of higher temperatures in the peak winter period. It shows that the model consistently underestimates the *wtd*, both in winter and summer. The observed *wtd* exhibits much lower values mostly during winter, and occasionally, positive *wtd*s are observed during summer.

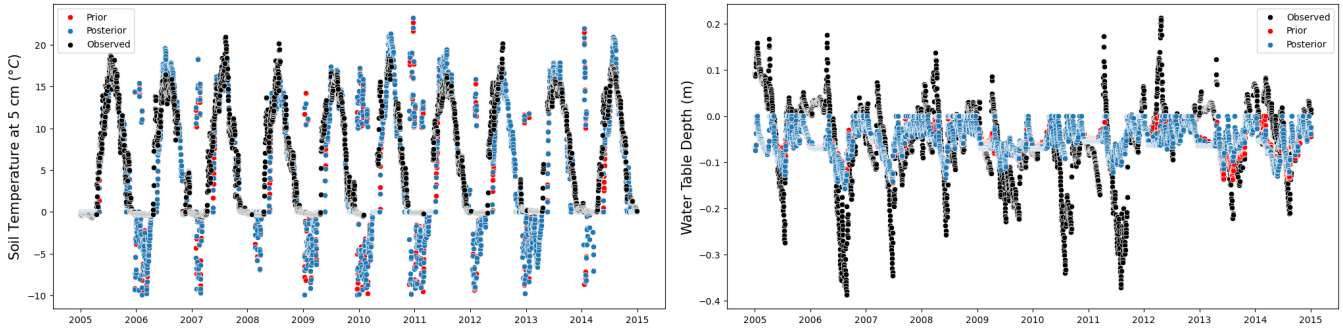

(a) Observed vs modelled soil temperature (°C) at 5 cm. (b) Observed vs modelled soil water table depth (m)

Figure S4. Time series examination of the observed vs. prior and posterior values of closely related components of CH_4 flux at Siikaneva. Figure (a) shows the soil temperature at a 5 cm depth, and Fig. (b) shows the soil water table depth.

S5 Sensitivity of the model to input variables

To examine the sensitivity of LPJ-GUESS to the input variables before and after the optimisation, we conducted a sensitivity analysis (Fig. S5). Sensitivity was estimated by increasing the air temperature by one degree and swr and precipitation by 10 % of their original site estimation. The estimates of sensitivity have been consistently low for the posterior estimates, with an 82 % decrease in sensitivity to swr and a 114 % decrease in sensitivity to precipitation. In the case of temperature, the reduction observed was relatively smaller, around 15 %.

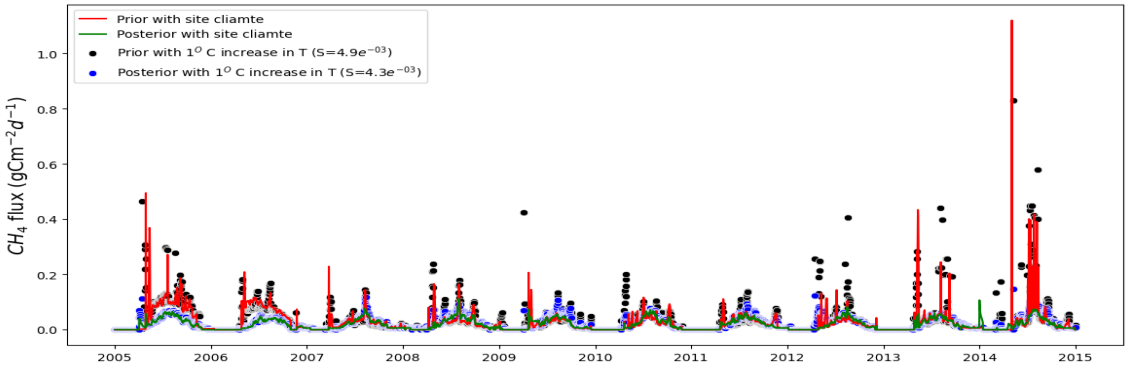

(a) Model sensitivity to air temperature

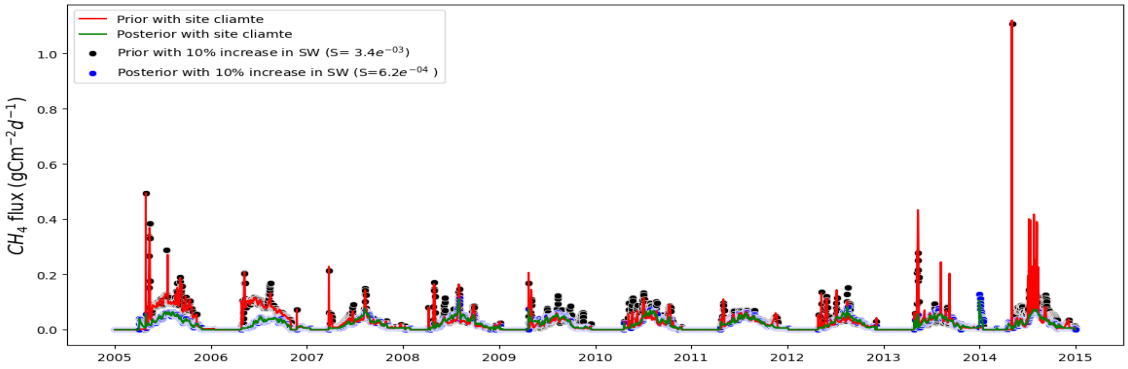

(b) Model sensitivity to short wave radiation

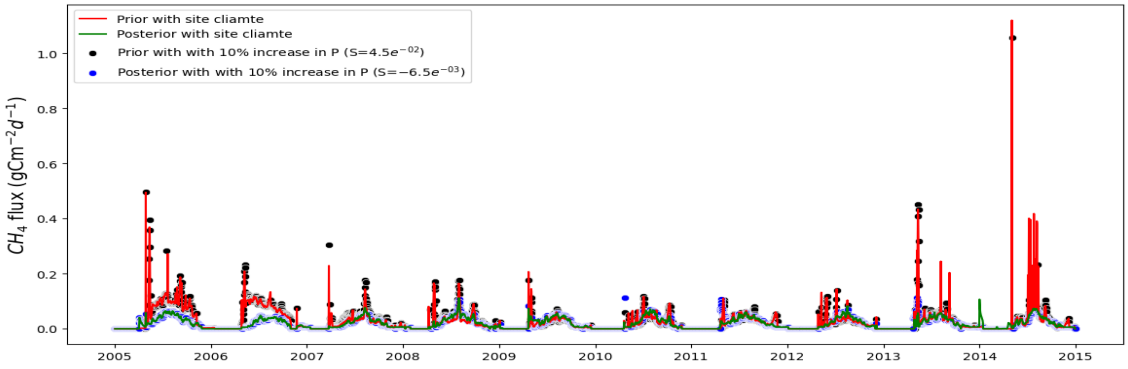

(c) Model sensitivity to precipitation

Figure S5. Prior and posterior model sensitivity to the input variables. The letter 'S' against the prior and posterior represents the sensitivity of each to the corresponding variable.

References

Bonan, G. B., Oleson, K. W., Vertenstein, M., Levis, S., Zeng, X., Dai, Y., Dickinson, R. E., and Yang, Z.-L.: The land surface climatology of the Community Land Model coupled to the NCAR Community Climate Model, Journal of climate, 15, 3123–3149, 2002.

Chadburn, S., Burke, E., Essery, R., Boike, J., Langer, M., Heikenfeld, M., Cox, P., and Friedlingstein, P.: An improved representation of physical permafrost dynamics in the JULES land-surface model, Geoscientific Model Development, 8, 1493–1508, 2015.

Frolking, S., Roulet, N. T., Moore, T. R., Richard, P. J., Lavoie, M., and Muller, S. D.: Modeling northern peatland decomposition and peat accumulation, Ecosystems, 4, 479–498, 2001.

Frolking, S., Roulet, N. T., Tuittila, E., Bubier, J. L., Quillet, A., Talbot, J., and Richard, P.: A new model of Holocene peatland net primary production, decomposition, water balance, and peat accumulation, Earth System Dynamics, 1, 1–21, 2010.

Granberg, G., Grip, H., Löfvenius, M. O., Sundh, I., Svensson, B., and Nilsson, M.: A simple model for simulation of water content, soil frost, and soil temperatures in boreal mixed mires, Water resources research, 35, 3771–3782, 1999.

Parton, W.: The CENTURY model, in: Evaluation of soil organic matter models, pp. 283–291, Springer, 1996.

Smith, B., Wårlind, D., Arneth, A., Hickler, T., Leadley, P., Siltberg, J., and Zaehle, S.: Implications of incorporating N cycling and N limitations on primary production in an individual-based dynamic vegetation model, Biogeosciences, 11, 2027–2054, 2014.

Wania, R., Ross, I., and Prentice, I. C.: Integrating peatlands and permafrost into a dynamic global vegetation model: 1. Evaluation and sensitivity of physical land surface processes, Global Biogeochemical Cycles, 23, 2009a.

Wania, R., Ross, I., and Prentice, I.: Integrating peatlands and permafrost into a dynamic global vegetation model: 2. Evaluation and sensitivity of vegetation and carbon cycle processes, Global Biogeochemical Cycles, 23, 2009b.

Wania, R., Ross, I., and Prentice, I.: Implementation and evaluation of a new methane model within a dynamic global vegetation model: LPJ-WHyMe v1. 3.1, Geoscientific Model Development, 3, 565–584, 2010.